Temporal ghost imaging with pseudo-thermal speckle light

2017 J. Opt. 19 024001

(http://iopscience.iop.org/2040-8986/19/2/024001)

IOP Publishing Journal of Optics
J. Opt. 19 (2017) 024001 (5pp) doi:10.1088/2040-8986/aa5328

Temporal ghost imaging with pseudo-thermal speckle light

Fabrice Devaux[1], Kien Phan Huy[1], Séverine Denis[1], Eric Lantz[1] and Paul-Antoine Moreau[2]

[1] Institut FEMTO-ST, Département d'Optique P. M. Duffieux, UMR 6174 CNRS Université Bourgogne Franche-Comté, 15b Avenue des Montboucons, F-25030 Besançon, France
[2] Centre for Quantum Photonics, H. H. Wills Physics Laboratory and Department of Electrical and Electronic Engineering, University of Bristol, Merchant Venturers Building, Woodland Road, Bristol BS8 1UB, UK

E-mail: fabrice.devaux@univ-fcomte.fr

Received 10 November 2016, revised 6 December 2016
Accepted for publication 12 December 2016
Published 29 December 2016

Abstract

We report ghost imaging of a single non-reproducible temporal signal with kHz resolution by using pseudo-thermal speckle light patterns and a single detector array with a million of pixels working without any temporal resolution. A set of speckle patterns is generated deterministically at a sampling rate of tens kHz, multiplied by the temporal signal and time integrated in a single shot by the camera. The temporal information is retrieved by computing the spatial intensity correlations between this time integrated image and each speckle pattern of the set.

Keywords: ghost imaging, temporal ghost imaging, data processing by optical means, speckle, statistical optics

(Some figures may appear in colour only in the online journal)

1. Introduction

With the advent of laser sources in the early 1960s and their application in many research fields, some phenomena inherent to coherency of lasers were evidenced such as the speckle phenomenon [1]. Very quickly, the scientific community investigated this phenomenon [2] either to minimize its effects or in order to take advantage of its properties for different metrology applications [3]. Since then, speckle applications have increased and thanks to constant advances in technology, new developments are proposed [4, 5].

Thus, exploitation of the statistical properties of speckle is the cause of fascinating new applications such as ghost imaging which is a way to form images of an object with a single point detector (SPD) that does not have spatial resolution. The initial works used the quantum nature of entanglement of a two-photons state, where photons of a pair are spatially correlated, to detect temporal coincidences [6]. While one of the photons passing through the object was detected by a photon counter with no spatial resolution, its twin photon was detected with spatial resolution by scanning the transverse plane with a single detector. Then, the object image was reconstructed by computing the correlation between both detectors. Later, similar experiments exploiting the temporal correlations of the intensity fluctuations of classical light [7] or pseudo-thermal speckle light [8] were proposed, showing that entanglement was not necessary to ghost imaging.

By taking into account space–time duality in optics, the extension of the results of spatial ghost imaging to the time domain has been investigated with different kinds of light source [9–13]. For all proposed arrangements, the light emitted by the sources was split into two arms, called 'reference' and 'test' arms. While in the test arm the light was transmitted through a 'time object' and detected with a slow SPD that can not properly resolve the time object, in the reference arm the light, that did not interact with the temporal object, was detected with a fast SPD. As for spatial ghost imaging, the temporal object was reconstructed by measuring the correlations of the temporal intensity fluctuations or the temporal coincidences between the two arms. In [13], measurements over several thousands copies of the temporal signal were necessary to retrieve an embedded binary signal with a good signal-to-noise ratio (SNR). The extension of

spatial ghost imaging to the time domain looks attractive for dynamic imaging of ultra-fast waveforms with high resolution. However, the method used in [13] requires thousands of realizations of the same temporal signal, limiting the current applications to the detection of synchronized and reproducible signals [14]. This is in contrast with the original concept of spatial ghost imaging, where the object is unique, but multiplied in the time domain by a random modulation, different from one pixel to another, leading to multiplexing in this time domain.

Recently, we have proposed a different scheme which is the exact space–time transposition of computational ghost imaging [15] and of wavelength-multiplexing ghost imaging [16]. In this experiment, a single complex temporal signal is measured in single-shot with a detector array without any temporal resolution [17]. To achieve this, the temporal information is multiplexed in the spatial domain by multiplying it with computer-generated random images. As a result the temporal information is copied and transferred to the spatial domain. As the single shot is taken with a long exposure time, all the images are integrated by the camera. Although the temporal information seems to be lost, it is embedded in the time integrated image and it is retrieved by computing spatial correlations between the time integrated image and the computer-generated random images. This operation transfers the information back from the spatial domain to the temporal one. We emphasize that this method allows to perform temporal ghost imaging without synchronization or replication of the temporal signal [13] with a single detector array with thousands pixels that has no temporal resolution. Indeed, as for the original computational ghost imaging arrangement [15], the use of pre-computing and reproducible random binary patterns prevent us to use a second array detector with a temporal resolution. Experiments were performed with monochrome images or color images to reconstruct either a single temporal signal or wavelength-multiplexed temporal signals, respectively. Currently, the main drawback of our method is its slowness (sampling rate of few Hz) which was imposed by the devices used to display the random patterns and to generate the temporal signals.

In the present paper, we report the first experimental demonstration of temporal ghost imaging with pseudo-thermal speckle patterns that allows the retrieval of a single non-reproducible temporal signal with kHz resolution. The signal reconstruction is performed by a single shot, spatially multiplexed, measurement of the temporal fluctuation of spatial intensity correlations of speckle patterns generated at tens of kHz and modulated by the temporal signal to detect. Like in [17], and because speckle patterns are generated deterministically, images are recorded and time integrated with a single detector array with a million of pixels used without any temporal resolution.

2. Experimental setup, measurement protocol and results

Figure 1(a) illustrates the experimental setup. To generate deterministically a basis of speckle patterns, a 543 nm CW He–Ne laser beam illuminates and scans the surface of a thin static scattering medium (SSM) by means of an acousto-optic deflector (AOD). The AOD is used in the Bragg configuration that gives a single, first diffraction order output beam, whose intensity and deflection angle are directly controlled with a variable radio-frequency (RF) driver. With our device, the RF carrier can be tuned in the range 40–100 MHz by an analog signal through the frequency modulation input (0–10 V FM in) which allows a deflection angle amplitude of 48 mrad in random access or raster scan mode. In order to control the deflection angle accurately at a kHz rate, a staircase waveform signal (figure 1(b)) is delivered by a programmable arbitrary wave generator (AWG) linked to a computer with a GPIB cable and controlled by a graphical user interface (GUI). The intensity of the first diffraction order is controlled with a DC supply connected to the 0–5 V amplitude modulation input (0–5 V AM in). Images of the objective speckle patterns are acquired with a compact CMOS USB2.0 camera (IDS UI-1640C, 1280 × 1024 pixels) on a 8 bits gray scale. We emphasize that there is no objective between the detector array and the SSM and the position of the camera is adjusted such as the whole detector array is illuminated uniformly by the speckle patterns whatever the deflection angle of the laser beam. We also point out that our arrangement requires a single detector array because the scattering medium is static. So, the speckle patterns can be generated deterministically and reproduced with accuracy.

Because of the laser beam divergence, the tuning of the deflection angle with a voltage step greater than or equal to $\Delta U_{\mathrm{AWG}} = 0.2$ V allows the generation of fully uncorrelated speckle patterns, providing the basis of independent random patterns required for the temporal ghost imaging protocol. This protocol is similar to that described in [17], except that the basis of K computed-random binary patterns is replaced by a basis of K speckle patterns. Let us name X this basis.

First, the protocol learning step consists in taking an image, with the camera, of each speckle pattern of the basis generated for a specific deflection angle. Figure 2(a) shows a typical image of a single speckle pattern and figure 2(b) shows the corresponding probability distribution of the pixel levels when the mean level of the background noise is subtracted. From these images, the mean and the variance of the speckles are calculated: $\langle X_k \rangle = 11 \pm 2$ and $\sigma^2_{X_k} = 122 \pm 32$. These values give a contrast ratio of the speckle patterns of 1.01 ± 0.04 and the good agreement of the probability distribution of the pixel levels with an exponential function (black dashed curve in figure 2(b)) shows that the statistical properties of speckles correspond to fully resolved pseudo-thermal light [4]. Figures 2(e) and (f) depict typical correlation function of a speckle pattern and cross-correlation function between two consecutive patterns of the set, respectively. The mean level of the cross-correlation function clearly shows that patterns of the set are independent. As any movement or vibration of the SSM, fluctuation of the laser wavelength or drift of the AOD will induce translation or variation of the speckle patterns, we verified that the stability of these components allows reproducibility of the speckle patterns during several hours.

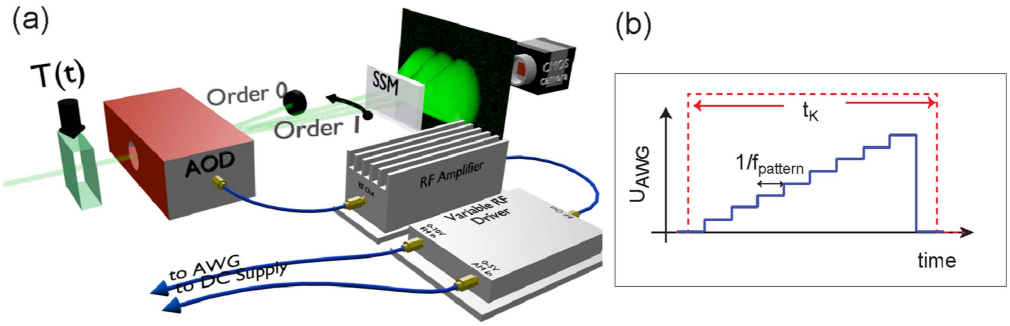

Figure 1. (a) Experimental setup: a static scattering medium (SSM) is illuminated with a 543 nm CW He–Ne laser beam. The basis of independent and reproducible speckle patterns is obtained by scanning the SSM with the laser beam by means of an acousto-optic deflector (AOD) controlled by a variable radio-frequency (RF) driver. The RF carrier (i.e. the deflection angle of the first diffraction order) is adjusted through the 0–10 V input with a signal delivered by a programmable arbitrary wave generator (AWG) which is controlled by a graphical user interface (GUI). The temporal signal $T(t)$ is symbolized by a device or a phenomenon that modulates the intensity of the laser beam. (b) Typical staircase waveform delivered by the AWG to generate successively eight speckle patterns and the red dashed curve represents the duration t_K of the signal delivered by the AWG.

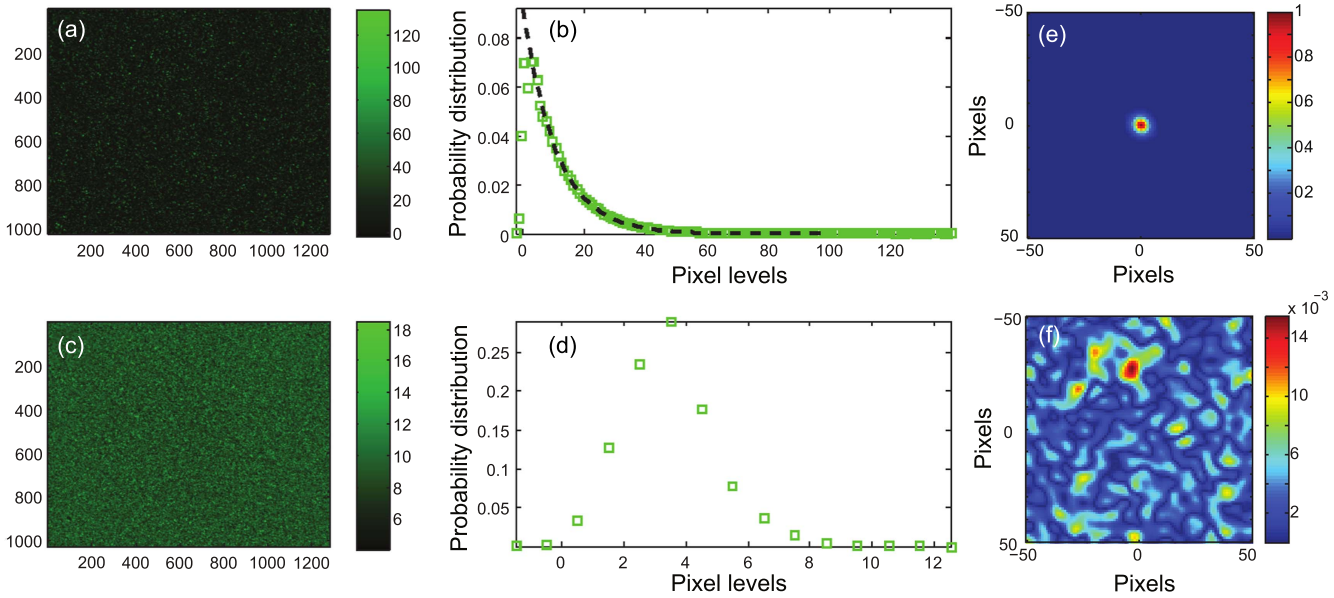

Figure 2. Images and distribution density of the pixel levels of: (a) and (b) a single speckle pattern, (c) and (d) a ghost image where a temporal signal is embedded. The dashed black curve in (b) corresponds to the exponential probability function of mean 11. (e) Autocorrelation function of a speckle pattern. (f) Cross-correlation function between two consecutive patterns of the set.

In the second step of the protocol, the same K speckle patterns are sequentially generated by applying to the AOD a unique staircase waveform delivered by the AWG at the frequency f_{pattern} during a time t_K (see figure 1(b)). During this time, the temporal signal, named $T(t)$ ($0 \leqslant T(t) \leqslant 1$) drives a device modulating linearly the intensity of the laser beam and therefore the intensity of the speckle patterns that are time-integrated by the camera with an exposure time $t_{\text{cam}} \gg t_K$. As we have investigated several methods and devices to address the temporal signal (with an electro-optic modulator like in [17], with the DC supply input of the RF driver or with the GUI interface), we would like to stress that any device or phenomenon providing intensity modulation of light is convenient for the protocol. Of course and because of a simple multiplication, the speckle pattern could also be generated before the temporal object as in [17] and an eventual transmission could occur after this object, inasmuch as spatial multiplexing is preserved. We also emphasize that this protocol is completely insensitive to any temporal distortion due to this transmission. Figure 2(c) shows a typical time-integrated image with an embedded temporal signal ($t_{\text{cam}} = 500$ ms, $t_K = 1$ ms, $K = 24$ and $f_{\text{pattern}} = \frac{K}{t_K} = 24$ kHz). Figure 2(d) shows the corresponding distribution of the pixel levels. The mean level of the time integrated images is smaller than the mean level of the single speckle images because the SSM is illuminated with a longer time for acquisition of the individual speckle patterns. The time-integrated image, named S, is given by:

$$S_{ij} = \frac{1}{\gamma} \sum_{k=1}^{K} T(k) X_{k,ij}, \tag{1}$$

where S_{ij} and $X_{k,ij}$ are the levels of the pixel of coordinates (i, j) in the images S and X_k, respectively. $T(k)$ is the value of the

temporal signal at the time when the kth speckle is generated. γ is a normalization coefficient corresponding to the ratio between the illumination durations of the SSM when the X_k and S images are recorded. As in [17], the temporal signal is reconstructed by calculating the intensity correlations between the time integrated image S and the K images X of the speckle patterns. The value of $T(k_0)$ at the 'time' k_0 is estimated by (a hat means 'estimator of'):

$$\hat{T}(k_0) = \gamma \frac{\sum_{i=1}^{N_x}\sum_{j=1}^{N_y}(S_{ij} - \overline{S})(X_{k_0,ij} - \overline{X}_{k_0})}{\sum_{i=1}^{N_x}\sum_{j=1}^{N_y}(X_{k_0,ij} - \overline{X}_{k_0})^2}, \qquad (2)$$

where $\overline{S}$ and $\overline{X}_{k_0}$ are the arithmetic mean levels of the related images. N_x and N_y are the numbers of pixels in the images along the x and y dimensions. With numerical simulations, we verified previously that the SNR is given theoretically by (see supplement material of [17]):

$$\mathrm{SNR}[T(k_0)] = \frac{T(k_0)}{\sigma_{T(k_0)}} = \sqrt{\frac{N_{\mathrm{eff}}}{\sum_{k=1,k\neq k_0}^{K} T^2(k)}}\, T(k_0)$$
$$\geqslant \sqrt{\frac{N_{\mathrm{eff}}}{K-1}}\, T(k_0), \qquad (3)$$

where N_{eff} represents the total number of independent spatial modes in the recorded image of a single speckle pattern. Typically, from the FWHM of the autocorrelation peak of a speckle pattern (figure 2(e)) we have estimated that a speckle (i.e. a spatial mode) covers an area of 23 ± 1 pixels of the camera : $N_{\mathrm{eff}} \backsimeq 5.7 \times 10^4$. For $K = 24$ and $T = 1$, it gives a theoretical SNRth $= 50 \pm 1$. To measure the SNR, we applied the protocol described above and speckle patterns were time-integrated by the camera with $T = 1$ during the entire exposure time. The protocol was repeated for different values of K and t_K. Then, the transmission coefficient T was calculated using equation (2) and the SNR was deduced from the fluctuations of the measured values of T. This measure was repeated several times in order to estimate the uncertainties. Figure 3 presents the measured SNR as a function of K for two different values of t_K : 1 ms (red square) and 3 ms (green square). In both cases, error bars are deduced from measurements. To compare, the blue dashed curve represents the theoretical SNRth calculated with equation (3). We can observe that while the measured SNR is in agreement with the theoretical values for $t_K = 3$ ms, it becomes much smaller than the theoretical value when K increases for $t_K = 1$ ms. Indeed, when K increases, f_{pattern} increases too and the 6.5 μs access time of the AOD becomes of the same order of magnitude as the illumination time of the SSM when a speckle pattern is generated. For example, with $f_{\mathrm{pattern}} =$ 24 kHz, the laser beam illuminates the SSM during 42 μs to generate a speckle pattern. However, the transition time between the successive deflection angles of the laser beam represents a quarter of this duration. Consequently, this motion of the laser beam at the surface of the SSM adds background noise that deteriorates the statistical properties of the speckle patterns and the SNR.

We present now the experimental results. Figures 4(a) and (b) show two kinds of reconstructed signals. The first one is a random binary word of 24 bits generated at the frequency

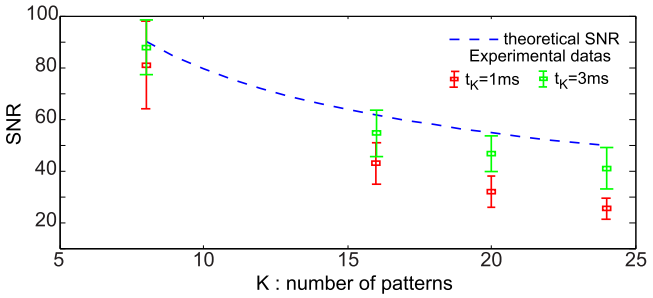

Figure 3. SNR as a function of the number K of time-intergrated speckle patterns. The blue dashed curve corresponds to the theoretical SNRth calculated with equation (3) and experimental data are represented by the red and green squares. They respectively correspond to 1 and 3 ms durations of the voltage of the pulses trains delivered by the AWG. The error bars are deduced form measurements.

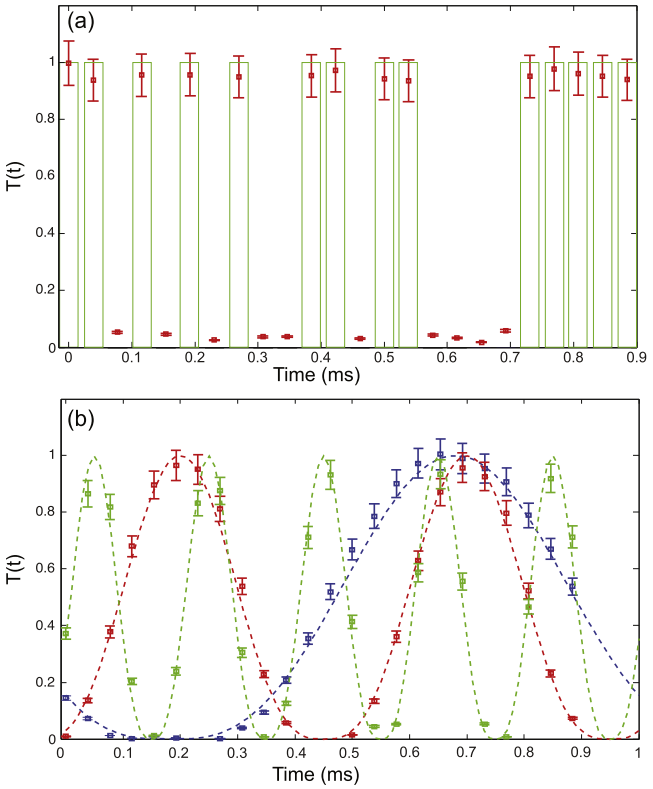

Figure 4. Results: (a) reconstructed random binary word of 24 bits at $f_{\mathrm{pattern}} = 24$ kHz. Green bars show the original signals. (b) Reconstructed periodic signals of frequencies 1, 2 and 5 kHz (respectively blue, red and green squares) sampled at $f_{\mathrm{pattern}} = 24$ kHz. The error bars are deduced from the measured SNR and the dotted curves show the original signals.

$f_{\mathrm{pattern}} = 24$ kHz with the GUI interface. This binary signal modulates directly the amplitude of the pulses train delivered by the AWG. When the kth bit equals '1', the kth speckle pattern is generated with the corresponding voltage $U_{\mathrm{AWG}}(k)$ and when it equals '0', $U_{\mathrm{AWG}}(k) = 0$ and the corresponding speckle pattern is not generated. Indeed, when $U_{\mathrm{AWG}} = 0\ V$, the first order diffracted beam is spatially filtered and does not illuminate the SSM. Then, temporal fluctuations of the spatial

correlations between the time-integrated image and the 24 images of the speckle patterns basis are calculated with equation (2). In figure 4(a) we can observe that the original signal represented by the green bars is reconstructed experimentally (red squares) with a good accuracy. Note that the spatial correlations between the ghost image and the missing patterns (corresponding to bits '0') are almost null, which clearly shows the independence of the speckle patterns. Figure 4(b) shows single shot measurements of non synchronized periodic signals of frequency 1, 2 and 5 kHz (respectively blue, red and green squares) sampled with the speckle patterns at the frequency $f_{\text{pattern}} = 24$ kHz. Here, the temporal signal is delivered by a wave function generator driving a device that modulates the transmission ($0 \leqslant T(t) \leqslant 1$) of the laser beam at the input of the AOD (see figure 1). The original signals are represented by the dashed curves (only phases of these curves are adjusted to fit the experimental data). For all experimental results the error bars are deduced from the measured SNR when $f_{\text{pattern}} = 24$ kHz.

3. Conclusion

To summarize, these experiments represent the first demonstration of the exact space–time transposition of spatial ghost imaging with pseudo-thermal speckle light. Unique and non reproducible time objects are reconstructed with a very good accuracy by multiplying them with independent and reproducible speckle patterns with a very large number of independent spatial modes. This method ensures spatial multiplexing of temporal intensity correlations before detection of the time integrated images of the speckle patterns with a camera that has no temporal resolution. When compared to the recent experimental demonstrations of temporal ghost imaging, the main advantages of our system consist first in the replacement of the need of thousands synchronized replica of the temporal signal required in [13] by the use of a detector array with a million pixels to acquire an unique non reproducible temporal signal. Moreover, our method is also in principle immune to dispersion or temporal distortion and implies a spatial multiplexing that must be preserved between the temporal object and the detector. This could be obtained by using a bundle of fibers and, importantly because the images in both the learning and integration steps are acquired after the transmission, any spatial mixing in the transmission would not have detrimental consequences if it is deterministic and does not change the number of spatial modes. Secondly, the resolution is greatly improved, from Hz to tens of kHz, with respect to our previous device for computational temporal ghost imaging [17]. Our results also demonstrate that deterministic speckle patterns with many spatial modes can be quickly controlled and addressed. Consequently, performances of our experiment, which are currently limited by the 6.5 μs access time of the AOD, could be seriously improved using spatial multiplexing of temporally modulated light sources, like 2D VCSELs array [18], to illuminate the SSM with a rate up to 8 GHz. It would be also possible to retrieve other signals affecting the laser beam properties, like phase or wavelength, by modifying the first, learning step of the protocol.

Acknowledgments

This work was supported by the Labex ACTION program (ANR-11-LABX-0001-01).

References

[1] Allen L and Jones D G C 1963 An analysis of the granularity of scattered optical maser light *Phys. Lett.* **7** 321–3
[2] Goodman J W 1975 Probability density function of the sum of *N* partially correlated speckle patterns *Opt. Commun.* **13** 244–7
[3] Dainty J C 1975 *Laser Speckle and Related Phenomena* (*Topics in Applied Physics* vol 9) (Berlin: Springer)
[4] Goodman J W 2007 *Speckle Phenomena in Optics: Theory and Applications* (Englewood, CO: Roberts and Company Publishers)
[5] Kaufmann G H (ed) 2011 *Advances in Speckle Metrology and Related Techniques* (New York: Wiley-VCH)
[6] Pittman T B, Shih Y H, Strekalov D V and Sergienko A V 1995 Optical imaging by means of two-photon quantum entanglement *Phys. Rev.* A **52** R3429–32
[7] Bennink R S, Bentley S J and Boyd R W 2002 Two-photon coincidence imaging with a classical source *Phys. Rev. Lett.* **89** 113601
[8] Ferri F, Magatti D, Gatti A, Bache M, Brambilla E and Lugiato L A 2005 High-resolution ghost image and ghost diffraction experiments with thermal light *Phys. Rev. Lett.* **94** 183602
[9] Shirai T, Setälä T and Friberg A T 2010 Temporal ghost imaging with classical non-stationary pulsed light *J. Opt. Soc. Am. B* **27** 2549–55
[10] Setälä T, Shirai T and Friberg A T 2010 Fractional Fourier transform in temporal ghost imaging with classical light *Phys. Rev.* A **82** 043813
[11] Cho K and Noh J 2012 Temporal ghost imaging of a time object, dispersion cancelation, and nonlocal time lens with bi-photon state *Opt. Commun.* **285** 1275–82
[12] Chen Z, Li H, Li Y, Shi J and Zeng G 2012 Temporal ghost imaging with a chaotic laser *Opt. Eng., Bellingham* **52** 076103
[13] Ryczkowski P, Barbier M, Friberg A T and Dudley J M 2016 Ghost imaging in the time domain *Nat. Photon.* **10** 167–70
[14] Faccio D 2016 Optical communications: temporal ghost imaging *Nat. Photon.* **10** 150–2
[15] Shapiro J H 2008 Computational ghost imaging *Phys. Rev.* A **78** 061802
[16] Zhang D-J, Li H-G, Zhao Q-L, Wang S, Wang H-B, Xiong J and Wang K 2015 Wavelength-multiplexing ghost imaging *Phys. Rev.* A **92** 013823
[17] Devaux F, Moreau P-A, Denis S and Lantz E 2016 Computational temporal ghost imaging *Optica* **3** 698–701
[18] Grabherr M, Intemann S, King R, Wabra S, Jäger R and Riedl M 2014 VCSEL arrays for high-aggregate bandwidth of up to 1.34Tbps *Proc. SPIE* **9001** 900105